Holographic stress-energy tensor near the Cauchy horizon inside a rotating black hole

Akihiro Ishibashi,[1,*] Kengo Maeda,[2,†] and Eric Mefford[3,‡]

[1]*Department of Physics, Kindai University, Higashi-Osaka 577-8502, Japan*
[2]*Faculty of Engineering, Shibaura Institute of Technology, Saitama 330-8570, Japan*
[3]*Department of Physics, University of California, Santa Barbara, California 93106, USA*

We investigate a stress-energy tensor for a conformal field theory (CFT) at strong coupling inside a small five-dimensional rotating Myers-Perry black hole with equal angular momenta by using the holographic method. As a gravitational dual, we perturbatively construct a black droplet solution by applying the "derivative expansion" method, generalizing the work of Haddad [Classical Quantum Gravity **29**, 245001 (2012)] and analytically compute the holographic stress-energy tensor for our solution. We find that the stress-energy tensor is finite at both the future and past outer (event) horizons and that the energy density is negative just outside the event horizons due to the Hawking effect. Furthermore, we apply the holographic method to the question of quantum instability of the Cauchy horizon since, by construction, our black droplet solution also admits a Cauchy horizon inside. We analytically show that the null-null component of the holographic stress-energy tensor negatively diverges at the Cauchy horizon, suggesting that a singularity appears there, in favor of strong cosmic censorship.

I. INTRODUCTION

One of the outstanding issues in gravity is understanding quantum effects in regions of large spacetime curvature. Although energy densities in typical classical fields such as electromagnetic fields are always non-negative, there have been a number of studies that show the appearance of negative energy density when quantum field effects are taken into account. For instance, it was shown (see, e.g., [1]) that the energy density for an observer falling into a singularity negatively diverges for some physical vacuum state. On the Cauchy horizon deep inside a charged black hole, the stress-energy tensor was calculated for a two-dimensional massless scalar field model, and the energy density diverges at the horizon [2]. Calculations of a conformal scalar field in Taub-NUT-type cosmologies show that the stress-energy tensor negatively diverges on the Cauchy horizon even though the curvature remains small [3]. However, most studies have been made for free massless scalar field models, and little attention has been given to strongly interacting field models such as conformal field theories (CFTs) at strong coupling.

The AdS/CFT duality [4] provides a powerful tool to investigate CFTs at strong coupling on a fixed curved background spacetime. According to the dictionary of the duality, a CFT at strong coupling on a fixed d-dimensional spacetime is dual to a gravitational theory in $(d+1)$-dimensional AdS spacetime with a timelike boundary

conformal to the d-dimensional spacetime. Motivated by the investigation of Hawking radiation in a model of a CFT at strong coupling, two types of black hole solutions were constructed in asymptotically locally AdS spacetimes [5–15]. One solution is called a "black funnel" in which there is a single connected horizon extending from the conformal boundary to an asymptotically planar horizon in the bulk, and it is dual to the thermal equilibrium Hartle-Hawking vacuum state of the boundary theory. The other is called a "black droplet" solution in which the horizon is disconnected from the planar horizon in the bulk, and it is dual to the Unruh vacuum state. In these models, negative energy density is observed outside the event horizon due to the Hawking effect. However, these solutions are quite complicated, and their construction has required numerical methods; hence, it is difficult to analyze the general properties of the stress-energy tensor inside the boundary black hole. It is then desirable to have some analytically constructed solutions for a black funnel/droplet. Recently, some attempts along this direction have been made by Haddad [16],[1] who, using a derivative expansion method, has constructed a five-dimensional *static* black droplet solution and computed the holographic stress-energy tensor for the corresponding dual quantum field in the background of a four-dimensional static black hole background [12] [see, also, for the lower-dimensional case ($d \leq 3$) [5,7,10]]. It is clearly interesting to generalize the line of research [12,16] performed for the static vacuum case to more

[*]akihiro@phys.kindai.ac.jp
[†]maeda302@sic.shibaura-it.ac.jp
[‡]mefford@physics.ucsb.edu

---

[1]Note that this expansion method is essentially the same as the one developed for the "blackfold approach" in [17]. See, also, e.g., [18] for further applications of this method.

general cases. In particular, including rotations would drastically change the causal structure inside the resultant black funnel/droplet motivating a study of the holographic consequences of strong coupling in quantum fields near the inner (Cauchy) horizon.

In this paper, we construct a *rotating* black droplet solution by generalizing the work [12]. In general, including rotation makes the relevant analysis significantly more complicated compared to the static case. For example, if one attempts to add a rotation to the model of [12] so that the corresponding boundary field lives in a four-dimensional Kerr black hole, which is already cohomogeneity-two, then one would have to construct a five-dimensional bulk black droplet by solving a cohomogeneity-three system. In order to avoid this technical difficulty, instead of trying to add a rotation to a five-dimensional black droplet, we attempt to construct a six-dimensional rotating black droplet solution dual to a five-dimensional field theory in the background of the rotating Myers-Perry black hole [19] with equal angular momenta, which is known to be cohomogeneity-one. In this case, the derivative expansion method enables us to reduce the bulk field equations to a set of ordinary differential equations, thereby making it possible to compute—analytically and explicitly within our expansion framework—the holographic stress-energy tensor for a CFT at strong coupling and large N inside the five-dimensional rotating black hole. In addition, since quantum field theories in odd dimensions are not well understood, it is of considerable interest to study the behavior of quantum fields in a five-dimensional spacetime. In fact, motivated from recent interests in five-dimensional conformal field theory (see, e.g., [14] for references), the six-dimensional rotating black droplet solutions dual to the rotating Myers-Perry black hole spacetime with equal angular momenta on the boundary were numerically constructed, and the holographic stress-energy tensor was derived in the region outside the event horizon [13,14].

Having two rotations, the rotating droplet solution admits not only an outer event horizon but also an inner (Cauchy) horizon. In this paper, we are primarily concerned with the properties of the holographic stress-energy tensor

inside the outer horizon and, in particular, investigating the quantum instability of the Cauchy horizon. We find that the null-null component of the stress-energy tensor diverges negatively near the Cauchy horizon, in agreement with the study of free massless scalar fields [2,3]. Our results suggest that the Cauchy horizon suffers from a quantum instability in favor of the strong cosmic censorship. As far as we know, this is the first example of applying the holographic method to study the Cauchy horizon instability due to quantum effects. We also find that negative energy appears just outside the outer horizon, describing particle creation by the Hawking effect. Nevertheless, there is no flux at infinity. This suggests that the dual phase corresponds to a transition from black funnels to black droplets and that it is reminiscent of soft condensed matter systems representing a transition from a fluidlike behavior to rigid behavior, just like a "jammed" state [13] (see, also, [15]).

The paper is organized as follows. In the next section, we describe our metric *Ansatz*, derive the equations of motion, and construct a rotating black droplet solution in six dimensions by using the derivative expansion method. In Sec. III, we perform an analytic computation of the holographic stress-energy tensor for a CFT at strong coupling and large N inside the five-dimensional rotating black hole on the boundary. In Sec. IV, we numerically check our results analytically obtained in the previous sections. Section V is devoted to summary and discussion.

II. DERIVATIVE EXPANSION METHOD

In this section, we derive the field equations following the derivative expansion method [16] and investigate general properties of the solution. Our bulk field equations are the six-dimensional vacuum Einstein equations with negative cosmological constant,

$$R_{\mu\nu} = -\frac{5}{L^2} g_{\mu\nu}, \tag{2.1}$$

where L is the AdS radius. We start with the following metric *Ansatz*:

$$d\bar{s}^2 = \left[\frac{L^2}{z^2 F(z)} - \frac{z^2}{L^2}\left(\frac{rF'(z)}{2F(z)}\right)^2\right]dz^2 + \frac{z^2 r\alpha(r,z)F'(z)}{L^2 F(z)}\{\sqrt{F(z)}dvdz - drdz\} + \frac{z^2}{L^2}\left[-F(z)\frac{f(r,z)}{h(r,z)}dv^2\right.$$

$$\left. + 2\sqrt{\frac{F(z)}{h(r,z)}}dvdr + \frac{r^2}{4}(d\theta^2 + \sin^2\theta d\phi^2) + r^2 h(r,z)\left(d\psi + \frac{\cos\theta}{2}d\phi - \sqrt{F(z)}\Omega(r,z)dv\right)^2\right],$$

$$f(r,z) = \left(1 - \frac{r_+^2(z)}{r^2}\right)\left(1 - \frac{\kappa^2 r_+^2(z)}{r^2}\right), \qquad h(r,z) = 1 + \frac{\kappa^2 r_+^4(z)}{r^4},$$

$$\Omega(r,z) = \frac{\kappa\sqrt{1 + \kappa^2}r_+^3(z)}{h(r,z)r^4}, \qquad F(z) = 1 - \frac{\mu^5}{z^5}, \tag{2.2}$$

where α is an unknown function of r and z determined later. In the limit $r_+ \to 0$ and $\alpha \to -1$, this metric reduces to the familiar planar Schwarzschild-AdS spacetime with horizon radius μ after performing the coordinate transformation, $v = t + r/\sqrt{F(z)}$. Furthermore, the metric at each $z =$ const hypersurface represents the cohomogeneity-one Myers-Perry black hole solution with equal angular momenta [19], where the outer and inner (Cauchy) horizons are located at $r = r_+$ and $r = \kappa r_+$ ($0 \le \kappa < 1$), respectively. So, the metric (2.2) represents a rotating black string embedded in the background planar Schwarzschild-AdS spacetime in which the horizon is extended along the z direction. The metric (2.2) itself does not satisfy Eqs. (2.1) and must be corrected order by order in derivatives. To this end, we write the metric as

$$ds^2 = d\bar{s}^2 + ds_{(\epsilon)}^2,$$

$$ds_{(\epsilon)}^2 = \sum_{n=1}^{\infty} \epsilon^n h_{\mu\nu}^{(n)}(r) dx^\mu dx^\nu, \qquad (2.3)$$

where ϵ is the formal derivative expansion parameter defined below, and $h_{\mu\nu}^{(n)}(r)$ is the nth correction of the metric determined by the Einstein equations (2.1). The derivative expansions are valid only when the horizon radius of the string is much smaller than the other scales,

$$r_+ \ll \mu \sim L. \qquad (2.4)$$

This implies that the background metric (2.2) changes very slowly along the z direction compared with the radial scale r_+. Thus, the contributions of the first and second derivatives with respect to the z direction to the Einstein

equations (2.1) are suppressed by a factor of r_+/L and $(r_+/L)^2$ [or similarly, r_+/μ and $(r_+/\mu)^2$].

Following Ref. [16], we shall expand the metric functions, F, r_+, and α in a series of $z - z_c$ around an arbitrary value z_c as

$$g(r, z) = g_c + \epsilon g_1(z - z_c) + \epsilon^2 g_2(z - z_c)^2 + \cdots, \qquad (2.5)$$

where $g(r, z)$ collectively denotes the metric functions such as F, r_+, and α, and the expansion coefficients are $g_n := \partial_z^n g(z_c)/n!$. Note that the expansion coefficients are functions of only r, but F_n and r_n are independent of r.

So, the Einstein equations (2.1) are formally modified to

$$r_c^2 R_{\mu\nu} = -5\epsilon^2 \frac{r_c^2}{L^2} g_{\mu\nu}, \qquad (2.6)$$

where $r_c = r_+(z_c)$. This implies that the effect of the cosmological constant appears at second order in the derivative expansion (2.5). Note that the derivative expansion parameter ϵ will be set to unity at the end of our calculations.

A. First order in derivatives

Substituting Eqs. (2.2) and (2.3) into Eqs. (2.6), one finds that the field equations (2.6) are satisfied at first order by

$$h_{\mu\nu}^{(1)}(r) = 0, \qquad (2.7)$$

provided that the following two equations with respect to $\alpha(r; z_c)$ are satisfied:

$$\alpha' + \frac{\alpha}{r} + \frac{(6F_c r_1 + F_1 r_c)r^8 + 24\kappa^2 r_1 F_c r_c^4 r^4 + \kappa^4 r_c^8(2F_c r_1 - F_1 r_c)}{4F_1 r_c r^3(r^4 + \kappa^2 r_c^4)^{3/2}} = 0,$$

$$\alpha'' + \left(\frac{1}{r} + \frac{4r^3}{r^4 + \kappa^2 r_c^4}\right)\alpha' - \left(\frac{1}{r^2} - \frac{4r^2}{r^4 + \kappa^2 r_c^4}\right)\alpha + \frac{3F_1 r^8 + 4\kappa^2 r_c^3(F_1 r_c - r_1 F_c)r^4 + \kappa^4 r_c^7(4F_c r_1 + F_1 r_c)}{F_1(r^4 + \kappa^2 r_c^4)^{5/2}} = 0. \qquad (2.8)$$

When

$$r_1 = \frac{r_c F_1}{2F_c} \qquad (2.9)$$

is satisfied, the solution α satisfying both two equations (2.8) is given by

$$\alpha(r; z_c) = -\frac{r^2}{\sqrt{r^4 + \kappa^2 r_c^4}} + \frac{C}{r}, \qquad (2.10)$$

where C is an integration constant. We discard the integration constant C because it can be eliminated by gauge transformation of $v \to v + C/\sqrt{F}$. In this case, the

$\kappa \to 0$ limit agrees with the nonrotating four-dimensional black string case [16].

B. Second order in derivatives

At second order $O(\epsilon^2)$, we make an *Ansatz* for the nonzero perturbed metric $h_{\mu\nu}^{(2)}$ as

$$h_{\mu\nu}^{(2)} dx^\mu dx^\nu = 2\gamma(r)\left(d\psi + \frac{\cos\theta}{2}d\phi\right)dv + h_{vv}(r)dv^2$$

$$+ 2h_{vr}(r)dvdr + h_{zz}(r)dz^2$$

$$+ \beta(r)\left(d\psi + \frac{\cos\theta}{2}d\phi\right)^2. \qquad (2.11)$$

We derive equations of motion for the metric functions above by substituting Eqs. (2.2), (2.3), and (2.11) into (2.6) and also using α given by (2.10) with r_c replaced by r_+. The equation of motion for h_{zz} is decoupled from the other variables as

$$-\frac{L^2 F_c^2 (r^2 - r_c^2)(r^2 - \kappa^2 r_c^2)(r^4 + \kappa^2 r_c^4)^3 z_c^{10}}{5r^2} h_{zz}'' - \frac{L^2 F_c^2 z_c^{10}\{3r^4 - r_c^2(1+\kappa^2)r^2 - \kappa^2 r_c^4\}(r^4 + \kappa^2 r_c^4)^3}{5r^3} h_{zz}' + \mathcal{P}(r) = 0,$$

$$(2.12)$$

where the source term $\mathcal{P}$ is explicitly given by Eq. (A1). The general solution includes two integral constants, one of which is determined by imposing the regularity on the horizon $r = r_c$. Then, we obtain the following analytic solution,

$$h_{zz} = -\frac{5r^2}{4L^2} + \frac{25\mu^{10}}{4L^2 F_c^2 z_c^{10}}\left(r^2 + \frac{\kappa^2 r_c^4 - r^4}{\sqrt{r^4 + \kappa^2 r_c^4}}\right) + \frac{5}{4L^2 F_c z_c^5}\{(z_c^5 + 5\mu^5)r^2 - 6\mu^5\sqrt{r^4 + \kappa^2 r_c^4}\}$$

$$+ \frac{15(1+\kappa^2)r_c^2\mu^5}{2L^2 F_c z_c^5}\ln(r^2 - \kappa^2 r_c^2) + C,$$

$$(2.13)$$

where C is the remaining integral constant. Hereafter, we discard this constant because it can be eliminated by making a gauge transformation [16]. We find that we can solve for h_{vr} in terms of the other variables, so we need only solve three coupled second order differential equations for $\gamma(r)$, $\beta(r)$, and h_{vv},

$$h_{vr} = \frac{\sqrt{F_c}(2r^2 - r_c^2(1+\kappa^2))r^3}{4(3r^4 - \kappa^2 r_c^4)\sqrt{r^4 + \kappa^2 r_c^4}}\beta' - \frac{\kappa\sqrt{1+\kappa^2}r_c^3 r^3}{(6r^4 - 2\kappa^2 r_c^4)\sqrt{r^4 + \kappa^2 r_c^4}}\gamma' - \frac{(3r^4 + \kappa^2 r_c^4)r^3}{4\sqrt{F_c}(3r^4 - \kappa^2 r_c^4)\sqrt{r^4 + \kappa^2 r_c^4}}h_{vv}'$$

$$+ \frac{\sqrt{F_c}r^2\{r_c^6\kappa^2(1+\kappa^2) + 3r_c^4\kappa^2 r^2 + r_c^2(1+\kappa^2)r^4 - r^6\}}{2(3r^4 - r_c^4\kappa^2)(r^4 + r_c^4\kappa^2)^{3/2}}\beta + \frac{\kappa\sqrt{1+\kappa^2}r_c^3 r^2}{(3r^4 - \kappa^2 r_c^4)\sqrt{r^4 + \kappa^2 r_c^4}}\gamma - \frac{r^2 h_{vv}}{2\sqrt{F_c}\sqrt{r^4 + \kappa^2 r_c^4}}$$

$$+ \frac{F_c^{3/2} z_c^4\{\kappa^2 r_c^4 - 2r_c^2(1+\kappa^2)r^2 + 3r^4\}r^3}{4L^4(3r^4 - \kappa^2 r_c^4)\sqrt{r^4 + \kappa^2 r_c^4}}h_{zz}' + \frac{5r^4}{8\sqrt{F_c}L^6 z_c^6(3r^4 - \kappa^2 r_c^4)(r^4 + \kappa^2 r_c^4)^{5/2}}$$

$$\times [8F_c^2 z_c^{10}(r^4 + \kappa^2 r_c^4)^2 r^4 + 5\{6r^{12} + 2\kappa^4 r_c^8 r^4 - 2\kappa^6 r_c^{12} + 3\kappa^4(1+\kappa^2)r_c^{10}r^2 + 2\kappa^2 r_c^4((1+\kappa^2)r_c^2 - \sqrt{r^4 + \kappa^2 r_c^4})r^6$$

$$- ((1+\kappa^2)r_c^2 + 6\sqrt{r^4 + \kappa^2 r_c^4})r^{10} + 2r_c^2(5\kappa^2 r_c^2 + 2(1+\kappa^2)\sqrt{r^4 + \kappa^2 r_c^4})r^8\}\mu^{10} - 8F_c^2 z_c^{10}(r^4 + \kappa^2 r_c^4)^2 r^4], \quad (2.14)$$

$$\sqrt{F_c}L^6 r^2(r^2 - r_c^2)(r^2 - \kappa^2 r_c^2)(3r^4 - \kappa^2 r_c^4)(r^4 + \kappa^2 r_c^4)^2\gamma'' + \sqrt{F_c}L^6 r(r^4 + \kappa^2 r_c^4)^2\{3r^8 - 3(1+\kappa^2)r_c^2 r^6$$

$$+ 2\kappa^2 r_c^4 r^4 - 7\kappa^2(1+\kappa^2)r_c^6 r^2 - r_c^8\kappa^4\}\gamma' - 4\sqrt{F_c}L^6(r^4 + \kappa^2 r_c^4)^3\{3r^4 - 3(1+\kappa^2)r_c^2 r^2 - \kappa^2 r_c^4\}\gamma$$

$$+ 2F_c L^6\kappa\sqrt{1+\kappa^2}r_c^3 r(r^4 + \kappa^2 r_c^4)^2\{r^4 - 2(1+\kappa^2)r_c^2 r^2 + \kappa^2 r_c^4\}\beta' - 8L^6\kappa^3\sqrt{1+\kappa^2}r_c^7 r^3(r^4 + \kappa^2 r_c^4)^2 h_{vv}'$$

$$+ 4F_c L^6\kappa\sqrt{1+\kappa^2}r_c^3(r^4 + \kappa^2 r_c^4)^2\{r^4 + 2(1+\kappa^2)r_c^2 r^2 + \kappa^2 r_c^4\}\beta$$

$$+ 4F_c^2 L^2 z_c^4\kappa\sqrt{1+\kappa^2}r_c^3 r^3(r^4 + \kappa^2 r_c^4)^2\{3r^4 - 2(1+\kappa^2)r_c^2 r^2 + \kappa^2 r_c^4\}h_{zz}' + \mathcal{S}(r) = 0, \quad (2.15)$$

$$- F_c L^6 r(r^2 - r_c^2)(r^2 - \kappa^2 r_c^2)(3r^4 - \kappa^2 r_c^4)(r^4 + \kappa^2 r_c^4)^2\beta'' + F_c L^6(r^4 + \kappa^2 r_c^4)^2\{3r^8 - 9(1+\kappa^2)r_c^2 r^6 + 6\kappa^2 r_c^4 r^4$$

$$- 5\kappa^2(1+\kappa^2)r_c^6 r^2 + 3r_c^8\kappa^4\}\beta' + 12F_c L^6 r(r^4 + \kappa^2 r_c^4)^3\{2r^2 + (1+\kappa^2)r_c^2\}\beta$$

$$- 8\sqrt{F_c}L^6\kappa\sqrt{1+\kappa^2}r_c^3 r^2(3r^4 + \kappa^2 r_c^4)(r^4 + \kappa^2 r_c^4)^2\gamma' - 8L^6\kappa^2 r_c^4 r^2(3r^4 + \kappa^2 r_c^4)(r^4 + \kappa^2 r_c^4)^2 h_{vv}'$$

$$+ 16\sqrt{F_c}L^6\kappa\sqrt{1+\kappa^2}r_c^3 r(3r^4 + \kappa^2 r_c^4)(r^4 + \kappa^2 r_c^4)^2\gamma$$

$$+ 8F_c^2 L^2\kappa^2 z_c^4 r_c^4 r^2(r^4 + \kappa^2 r_c^4)^2\{3r^4 - 2(1+\kappa^2)r_c^2 r^2 + \kappa^2 r_c^4\}h_{zz}' + \mathcal{R}(r) = 0, \quad (2.16)$$

$$- L^6 r^2 (r^2 - r_c^2)(r^2 - \kappa^2 r_c^2)(3r^4 - \kappa^2 r_c^4)(r^4 + \kappa^2 r_c^4)^2 h_{vv}''$$

$$- L^6 r(r^4 + \kappa^2 r_c^4)^2 \{9r^8 - 9(1 + \kappa^2)r_c^2 r^6 - 6\kappa^2 r_c^4 r^4 + 7\kappa^2(1 + \kappa^2)r_c^6 r^2 + \kappa^4 r_c^8\} h_{vv}'$$

$$- 2F_c L^6 (1 + \kappa^2) r_c^2 r^3 (r^4 + \kappa^2 r_c^4)^2 \{(1 + \kappa^2)r_c^2 - 2r^2\} \beta'$$

$$+ 4\sqrt{F_c} L^6 \kappa \sqrt{1 + \kappa^2} r_c^3 r (r^4 + \kappa^2 r_c^4)^2 \{3r^4 - (1 + \kappa^2)r_c^2 r^2 - \kappa^2 r_c^4\}(r\gamma' - 2\gamma)$$

$$- 4F_c L^6 (1 + \kappa^2) r_c^2 (r^4 + \kappa^2 r_c^4)^2 \{4r^4 - (1 + \kappa^2)r_c^2 r^2 - 2\kappa^2 r_c^4\} \beta$$

$$+ 2F_c^2 L^2 (1 + \kappa^2) r_c^2 z_c^4 r^3 (r^4 + \kappa^2 r_c^4)^2 \{3r^4 - 2(1 + \kappa^2)r_c^2 r^2 + \kappa^2 r_c^4\} h_{zz}' + \mathcal{Q}(r) = 0, \tag{2.17}$$

where $\mathcal{S}(r)$, $\mathcal{R}(r)$, and $\mathcal{Q}(r)$ are functions of r given by Eqs. (A2)–(A4) in the Appendix. From the other constraint equations, we obtain the coefficient r_2 as

$$r_2 = \frac{r_c(4F_2 F_c - F_1^2)}{8F_c^2}. \tag{2.18}$$

Combining Eqs. (2.9) and (2.18), we obtain

$$r_+(z) = r_0 \sqrt{F(z)} \tag{2.19}$$

up to second order in the derivative expansion, where r_0 is the radius of r_+ at the AdS boundary, $z \to \infty$. Just as in the nonrotating five-dimensional black string case [16], the droplet horizon shrinks to zero at the horizon of the planar Schwarzschild-AdS spacetime, ending on the horizon.

Equations (2.15)–(2.17) have a singular source term $\sim (r - r_c \kappa)^{-1}$ arising from h_{zz} in (2.13). This implies that γ, β, and h_{vv} can be expanded near the inner (Cauchy) horizon as

$$\gamma(r) \simeq \ln(r - \kappa r_c)\{a_0 + a_1(r - \kappa r_c) + a_2(r - \kappa r_c)^2 + \cdots\}$$
$$\qquad + d_0 + d_1(r - \kappa r_c) + \cdots,$$
$$\beta(r) \simeq \ln(r - \kappa r_c)\{b_0 + b_1(r - \kappa r_c) + b_2(r - \kappa r_c)^2 + \cdots\}$$
$$\qquad + e_0 + e_1(r - \kappa r_c) + \cdots,$$
$$h_{vv}(r) \simeq \ln(r - \kappa r_c)\{c_0 + c_1(r - \kappa r_c)$$
$$\qquad + c_2(r - \kappa r_c)^2 + \cdots\} + f_0 + f_1(r - \kappa r_c) + \cdots. \tag{2.20}$$

Note that we have assumed that the black droplet solution is nonextremal, i.e., $\kappa < 1$, in the expansion. Substituting these into Eqs. (2.15)–(2.17), we obtain all the coefficients provided that the coefficients c_0, d_0, e_0, f_0, e_1, and f_1 are given. This implies that six independent mode solutions exist for the second order differential equations (2.15)–(2.17). For the discussions in the next section, it suffices to obtain the relation between the leading order coefficients a_0, b_0, and c_0. The remaining subleading coefficients are determined by numerics in Sec. IV.

The leading coefficients a_0 and b_0 are determined by c_0 as

$$a_0 = -\frac{r_c \kappa \sqrt{1 + \kappa^2}\{2L^6 z_c c_0 + 15r_c^2(1 + \kappa^2)\mu^5 F_c\}}{2L^6 z_c(1 - \kappa^2)\sqrt{F_c}},$$

$$b_0 = \frac{r_c^2 \kappa^2 \{2L^6 z_c(1 + 3\kappa^2)c_0 + 15r_c^2(3 + 4\kappa^2 + \kappa^4)\mu^5 F_c\}}{2L^6(1 - \kappa^2)z_c F_c}. \tag{2.21}$$

By Eq. (2.14), we also find the asymptotic behavior of h_{vr} near the Cauchy horizon:

$$h_{vr} \simeq \frac{r_c \kappa^2 \{2L^6 z_c \kappa^2 c_0 + 15(1 + \kappa^2)r_c^2 \mu^5 F_c\}}{4L^6 z_c(1 - \kappa^2)\sqrt{1 + \kappa^2}\sqrt{F_c}(r - \kappa r_c)}. \tag{2.22}$$

C. The nonrotating case

In the nonrotating case ($\kappa = 0$), Eqs. (2.15) and (2.16), respectively, for γ and β are decoupled from the other variables, and we can set $\gamma = \beta = 0$. Furthermore, we obtain analytic expressions for h_{vv} and h_{vr} from Eqs. (2.13), (2.17), and (2.14):

$$h_{zz} = \frac{15r_c^2 \mu^5 \ln r}{L^2 F_c z_c^5},$$

$$h_{vv} = C_2 - \frac{C_1}{2r^2} - \frac{5\mu^5 F_c r_c^2}{L^6 z_c r^2}\{r_c^2 - (r^2 - 2r_c^2)\ln r\},$$

$$h_{vr} = \frac{-4C_2 L^6 z_c^6 + 5r_c^2 \mu^5(4z_c^5 + \mu^5) - 20r_c^2 \mu^5 z_c^5 F_c \ln r}{8L^6 z_c^6 \sqrt{F_c}}, \tag{2.23}$$

where C_1 and C_2 are constants that correspond to a global shift in the temperature as explained in [16], so we must set it to zero.

III. THE HOLOGRAPHIC STRESS-ENERGY TENSOR

In this section, we calculate the holographic stress-energy tensor using the prescription of [20], up to the second order in ϵ. In the six-dimensional bulk theory, the regularized action becomes

$$S = \frac{1}{16\pi G_6} \int_{\mathcal{M}} dx^6 \sqrt{-g} \left(R + \frac{30}{L^2} \right) + \frac{1}{8\pi G_6} \int_{\partial\mathcal{M}} dx^5 \sqrt{-q} K$$
$$+ \frac{1}{8\pi G_6} \int_{\partial\mathcal{M}} dx^5 \sqrt{-q} \left[\frac{4}{L} + \frac{L}{6} \mathcal{R} + \frac{L^3}{18} \right.$$
$$\left. \times \left(\mathcal{R}_{ab} \mathcal{R}^{ab} - \frac{5}{16} \mathcal{R}^2 \right) + \cdots \right], \tag{3.1}$$

where $\mathcal{R}$ is the Ricci scalar of the induced metric $q_{ab} = g_{ab} - n_a n_b$ at $z = z_c$ associated with the unit normal outward pointing vector n^a, and K is the trace of the extrinsic curvature defined below. Note that the first three terms in the second line are sufficient to cancel the divergences. Furthermore, the last two terms are at $O(\epsilon^4)$, since the induced metric is the vacuum Myers-Perry black hole [19] at zeroth order, i.e., $\mathcal{R}_{ab} = \mathcal{R} = O(\epsilon^2)$. Thus, the holographic stress-energy tensor T_{ab} given by $T_{ab} = (2/\sqrt{-q})\delta S/\delta q^{ab}$ becomes

$$T_{ab} = \frac{L}{8\pi G_6} \left[\frac{1}{3} E_{ab} - \frac{\epsilon}{L}(K_{ab} - q_{ab}K) - \frac{4\epsilon^2}{L^2} q_{ab} \right] + O(\epsilon^4), \tag{3.2}$$

where E_{ab} is the Einstein tensor of the induced metric q_{ab}, and K_{ab} is the extrinsic curvature defined by

$$K_{ab} = q_a{}^c \nabla_c n_b. \tag{3.3}$$

If the metric (2.3) is decomposed into

$$ds^2 = (N^2 + N_a N^a) dz^2 + 2N_a dx^a dz + q_{ab} dx^a dx^b. \tag{3.4}$$

K_{ab} is rewritten by

$$K_{ab} = \frac{1}{2N}(\partial_z q_{ab} - D_a N_b - D_b N_a), \tag{3.5}$$

where D_a is the covariant derivative with respect to the induced metric q_{ab}, and the lapse function N and the shift vector N_a are given by

$$N_v = \frac{5\alpha r\mu^5}{2L^2 z_c^4} + O(z_c^{-9}), \qquad N_r = -\frac{5\alpha r\mu^5}{2L^2 z_c^4} + O(z_c^{-9}),$$

the other components $= 0$,

$$N = \frac{L}{z_c \sqrt{F_c}} + O(\epsilon^2). \tag{3.6}$$

Note that $N_a = O(\epsilon)$, as it includes the derivative with respect to z from Eq. (2.2). Thus, if we expand q_{ab}, K_{ab}, and E_{ab} as

$$q_{ab} = q^{(0)}{}_{ab} + \epsilon^2 q^{(2)}{}_{ab} + \cdots,$$
$$K_{ab} = \epsilon K^{(1)}_{ab} + \epsilon^3 K^{(3)}_{ab} + \cdots,$$
$$E_{ab} = \epsilon^2 E^{(2)}_{ab} + \cdots, \tag{3.7}$$

$K^{(1)}_{ab}$ is determined by $q^{(0)}{}_{ab}$ as

$$K^{(1)}_{ab} = \frac{z_c \sqrt{F_c}}{2L}(\partial_z q^{(0)}{}_{ab} - \bar{D}_a N_b - \bar{D}_b N_a), \tag{3.8}$$

where $\bar{D}_a$ denotes the covariant derivative with respect to $q^{(0)}{}_{ab}$. Then, Eq. (3.2) reduces to

$$T_{ab} = \frac{\epsilon^2 L}{8\pi G_6} \left[\frac{1}{3} E^{(2)}_{ab} - \frac{1}{L}(K^{(1)}_{ab} - q^{(0)}_{ab}K^{(1)}) - \frac{4}{L^2} q^{(0)}_{ab} \right] + O(\epsilon^4). \tag{3.9}$$

This implies that the second order perturbation $h^{(2)}_{\mu\nu}$ contributes to the stress-energy tensor only through the Einstein tensor, up to $O(\epsilon^2)$.

First, we investigate the stress-energy tensor in the static case ($\kappa = 0$). Substitution of Eqs. (2.23) into Eq. (3.9) yields

$$T_{vv} = \epsilon^2 \cdot C \cdot \frac{4r^6 - 9r_c^2 r^4 + 5r_c^6}{r^6},$$
$$T_{vr} = \epsilon^2 \cdot C \cdot \frac{-4r^4 + 5r_c^2 r^2 + 5r_c^4}{r^4},$$
$$T_{rr} = \epsilon^2 \cdot C \cdot \frac{5(r^2 - r_c^2)}{r^2},$$
$$T_{\psi\psi} = \frac{2}{\cos\theta} T_{\psi\phi} = \epsilon^2 \cdot C \cdot \frac{r^4 - 5r_c^4}{r^2},$$
$$T_{\theta\theta} = T_{\phi\phi} = \epsilon^2 \cdot C \cdot \frac{r^4 - 5r_c^4}{4r^2}, \tag{3.10}$$

where $C = \mu^5/16\pi G_6 L^3 z_c^3$. It is easily checked that the conservation law $\bar{D}_a T^{ab} = 0$ is satisfied. Near the outer horizon $r = r_c$, negative energy density appears, i.e., $T_{vv} < 0 (r > r_c)$. This implies that due to the Hawking effect, pair creation of particles occurs near the horizon, and the negative energy particles are absorbed into the horizon. Nevertheless, there is no flux at null infinity. This is verified by checking that the (t, r) component of the stress-energy tensor in the original coordinate system (t, r) becomes zero at null infinity. This is due to strong coupling effects of the dual CFT in the boundary theory, just as in the five-dimensional case [12]. It is also immediately checked that the trace of our stress-energy tensor vanishes, in agreement with the general argument that odd-dimensional CFTs have a vanishing trace anomaly.

Next, we investigate the stress-energy tensor near the inner (Cauchy) horizon in the rotating case. Note that K_{ab} is

regular near the Cauchy horizon $r = \kappa r_c$ at $O(\epsilon)$ because $q^{(0)}{}_{ab}$ and the shift vector N_a are regular there. Thus, the dominant term of T_{ab} in Eq. (3.2) near the Cauchy horizon comes from the Einstein tensor E_{ab}. As shown in Eqs. (2.20)–(2.22), the second order metric h_{ab} diverges near the Cauchy horizon. So, the relevant [i.e., (r, r)] component of the Einstein tensor E_{ab} can be expanded as

$$E_{rr} = \frac{\epsilon^2}{z_c^3}\left[-\frac{15r_c^2(1+\kappa^2)\mu^5}{4L^4(r-r_c\kappa)^2} + \frac{C'}{r-\kappa r_c} + \cdots\right] + O(\epsilon^4),$$

(3.11)

where C' is a constant. As for the other components, the leading terms in order $O(\epsilon^2)$ behave as $1/(r - \kappa r_c)$ and, therefore, are irrelevant to the rest of our arguments.

The most striking feature is that E_{rr} in Eq. (3.11) negatively diverges at the Cauchy horizon. This implies that the null energy condition is strongly violated along the null direction ∂_r near the Cauchy horizon:

$$T_{rr} \simeq -\frac{5\epsilon^2 r_c^2(1+\kappa^2)\mu^5}{32\pi G_6 L^3 z_c^3(r-r_c\kappa)^2} \to -\infty. \quad (3.12)$$

Interestingly, this behavior is very similar to the case of the massless scalar field in two dimensions [2,3]; in both cases, the stress-energy tensor negatively diverges as $(r - \kappa r_c)^{-2}$.

IV. NUMERICAL RESULTS

When we add rotation to our droplets, we must solve the second order equations numerically. To account for the logarithmic divergences in β, γ, and h_{vv}, as well as the pole in h_{vr}, we make the following *Ansätze*,

$$\beta(r) = \beta_L(r)\ln(r-\kappa r_c) + \beta_1(r),$$
$$\gamma(r) = \gamma_L(r)\ln(r-\kappa r_c) + \gamma_1(r),$$
$$h_{vv}(r) = h_{vvL}(r)\ln(r-\kappa r_c) + h_{vv1}(r),$$
$$h_{vr}(r) = h_{vrL}(r)\ln(r-\kappa r_c) + \frac{r}{r-\kappa r_c}h_{vr1}(r). \quad (4.1)$$

In the last equation, the coefficient of $h_{vr1}(r)$ is required to have $h_{vv1}(r)$ vanish as r goes to infinity, matching the nonrotating case.

We insert these *Ansätze* into (2.14) and find eight equations to solve numerically—four from the coefficients of $\ln(r - \kappa r_c)$ involving only β_L, γ_L, h_{vvL}, and h_{vrL} and four remaining equations involving these variables as well as $\beta_1, \gamma_1, h_{vv1}, h_{vr1}$. It is numerically convenient to also set $L = 1$ and work in terms of a variable $R \equiv 1/r$ in order to impose boundary conditions at spatial infinity.

As we did in the analytic case, we can perform a series expansion in powers of $R - (\kappa r_c)^{-1}$ near the Cauchy horizon to find appropriate boundary conditions on our new metric functions,

$$X(R) = \sum_{i=0}^{\infty} x_i\left(R - \frac{1}{\kappa r_c}\right)^i, \quad (4.2)$$

where X refers collectively to $\{\beta_L, \gamma_L, h_{vvL}, h_{vrL}, \beta_1, \gamma_1, h_{vv1}, h_{vr1}\}$. This expansion reflects the fact that the divergences in β, γ, h_{vv} come only from a log term sourced by h_{zz}, and there is an extra divergence of $(r - \kappa r_c)^{-1}$ in h_{vr}. Inserting this expansion into our eight differential equations and solving order by order in $(R - \frac{1}{\kappa r_c})$ leads to the following boundary conditions,

$$h_{vrL}\left(R = \frac{1}{\kappa r_c}\right) = -\frac{\kappa(15(\kappa^2+1)(2\kappa^6+7\kappa^4+12\kappa^2+3)\mu^5 F_c r_c^2 + 2\kappa^2(5\kappa^4+14\kappa^2+5)z_c h_{vvL}(\frac{1}{\kappa r_c}))}{4(\kappa^2-1)^2(\kappa^2+1)^{3/2}\sqrt{F_c}z_c},$$

$$h'_{vvL}\left(\frac{1}{\kappa r_c}\right) = -\frac{\kappa(\kappa^2+1)r_c(15(\kappa^2+1)\mu^5 F_c r_c^2 + 2z_c h_{vvL}(\frac{1}{\kappa r_c}))}{(\kappa^2-1)z_c},$$

(4.3)

as well as the previously derived conditions, Eq. (2.21). Furthermore, the expansion leads to the following constraint at the horizon,

$$0 = 16\kappa(\kappa^2-1)r_c^2 z_c\left(2(\kappa^2+1)\sqrt{F_c}\gamma_1\left(\frac{1}{\kappa r_c}\right) + \sqrt{\kappa^2+1}h'_{vv1}\left(\frac{1}{\kappa r_c}\right)\right) + 5\kappa^2\mu^5 r_c^5(3(4\kappa^5 - 8\kappa^3 + 93\sqrt{\kappa^2+1}\kappa^2$$

$$+ 33\sqrt{\kappa^2+1} + 19\sqrt{\kappa^2+1}\kappa^6 + 63\sqrt{\kappa^2+1}\kappa^4 + 4\kappa)F_c - 20\kappa(\kappa^2-1)(\kappa^2 - 2\sqrt{\kappa^2+1}\kappa - 1))$$

$$- 4\left(\sqrt{\frac{1}{\kappa^2}+1} - \kappa^3\sqrt{\kappa^2+1}\right) - 8\sqrt{F_c}r_c z_c\left(3\kappa\left(\sqrt{\frac{1}{\kappa^2}+1} - \kappa^3\sqrt{\kappa^2+1}\right)\sqrt{F_c}\beta_1\left(\frac{1}{\kappa r_c}\right) - 2(\kappa^4-1)\gamma_1'\left(\frac{1}{\kappa r_c}\right)\right)$$

$$\times F_c z_c \beta_1'\left(\frac{1}{\kappa r_c}\right) + 2\kappa^2\sqrt{\kappa^2+1}(57\kappa^4 + 48\kappa^2 - 1)r_c^3 z_c h_{vvL}\left(\frac{1}{\kappa r_c}\right).$$
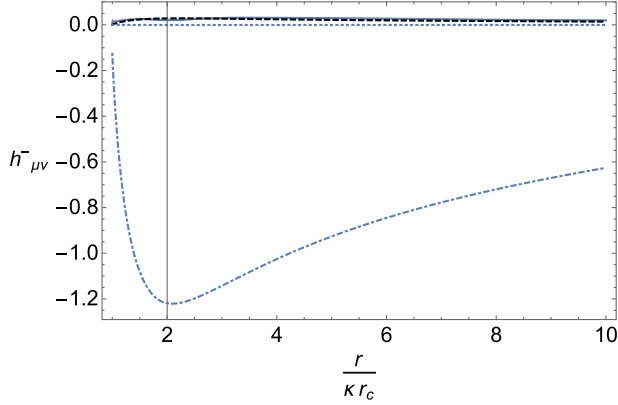
(4.4)

FIG. 1.   Here we plot the finite pieces of $h_{\mu\nu}(r)$ at $\mathcal{O}(\epsilon^2)$. The curves correspond to $\beta^-(r)$ (dotted), $\gamma^-(r)$ (dashed, black), $h_{vv}^-(r)$ (dot dashed), and $h_{vr}^-(r)$ (thick) for $r_c = 0.1$, $\mu = 1$, $\kappa = 0.2$, $z_c = (4\mu)^{1/5}$. Note that γ^- and h_{vr}^- nearly overlap, and β^- is much smaller than the other functions.

We can likewise perform a series expansion at spatial infinity in powers of R (recall that $R = 0$ corresponds to spatial infinity) to find appropriate boundary conditions. This leads to

$$\beta_L(0) = \gamma_L(0) = 0,$$

$$h_{vr1}(0) = \frac{-5(\kappa^2 + 1)\mu^5(F_c - 5)r_c^2 - 4z_c h_{vv1}(0)}{8\sqrt{F_c}z_c},$$

$$h_{vvL}(0) = \frac{5(\kappa^2 + 1)\mu^5 F_c r_c^2}{z_c},$$

$$h_{vrL}(0) = -\frac{5(\kappa^2 + 1)\mu^5 \sqrt{F_c}r_c^2}{2z_c},$$

$$\beta_1(0) = \frac{25\kappa^2\mu^{10}r_c^4}{2F_c z_c^6}, \qquad \gamma_1(0) = -\frac{25\kappa\sqrt{\kappa^2 + 1}\mu^{10}r_c^3}{2\sqrt{F_c}z_c^6}.$$

$$(4.5)$$

Note that these boundary conditions correspond to imposing a single constraint on the free parameters $c_0, d_0, f_0, e_1,$
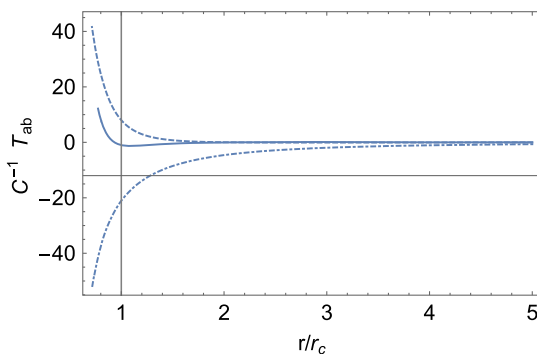
and f_1 in Eq. (2.20). Finally, there are a few boundary conditions which me must impose by hand. These are analogous to the constants C_1 and C_2 in Eq. (2.23). To smoothly match onto the nonrotating case, we choose $\beta_1(\frac{1}{\kappa r_c}) = \gamma_1(\frac{1}{\kappa r_c}) = 0$ and $h_{vv1}(0) = 0$. This choice is equivalent to imposing $d_0 = e_0 = f_0 = 0$.

These boundary conditions are not sufficient to ensure smooth solutions because the point $R = 3^{1/4}/(r_c\sqrt{\kappa})$ is a (regular) singular point of our differential equations. To accommodate this singularity, we used two numerical regions, $0 \leq R \leq \frac{3^{1/4}}{r_c\sqrt{\kappa}}$ and $\frac{3^{1/4}}{r_c\sqrt{\kappa}} < R < \frac{1}{\kappa r_c}$ (this is only necessary for $\kappa < \sqrt{3}$). We impose continuity of our functions and match the first derivatives of our functions at this point. Regularity of the differential equation, or similar smoothness of h_{vrL} and h_{vr1} at our singular point, amounts to two constraints. In total, we start with four free constants, $\beta_1(\frac{1}{\kappa r_c})$, $\gamma_1(\frac{1}{\kappa r_c})$, $h_{vvL}(\frac{1}{\kappa r_c})$, and $h_{vv1}(0)$ and fix three by hand to smoothly match onto the nonrotating solution. The final constant is fixed by consistency of the two constraints coming from the smoothness of h_{vr1}, h_{vrL}.

To find these numerical solutions, we use the Newton-Raphson method with pseudospectral collocation over a Chebyshev grid in the two numerical domains. In Fig. 1, we have plotted our solutions for $r_c = 0.1$, $\mu = 1$, $\kappa = 0.2$, $z_c = (4\mu)^{1/5}$ (reexpressed in terms of the original radial coordinate r). Importantly, we have included only the finite pieces of the solutions, subtracting off the divergent pieces. For example, using the notation of (2.20),

$$\beta^-(r) \equiv \beta(r) - b_0 \ln(r - \kappa r_c),$$
$$\gamma^- \equiv \gamma^-(r) - a_0 \ln(r - \kappa r_c),$$
$$h_{vv}^-(r) = h_{vv}(r) - c_0 \ln(r - \kappa r_c) \qquad (4.6)$$

and similarly for $h_{vr}^-(r)$.

We have also plotted the nonvanishing components of the stress-energy tensor for this solution in Fig. 2. We have
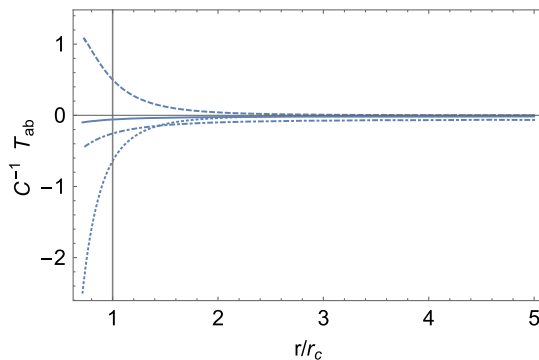

FIG. 2.   Here we plot the components of the holographic stress-energy tensor for the same parameters as Fig. 1 with $\theta = \pi/2$ and $z_c = (10^8\mu)^{1/5}$. In the left plot, we show T_{vr} (dashed), T_{rr} (dot dashed), and T_{vv} (thick). On the right, we show $T_{\psi r}$ (dotted), $T_{\psi v}$ (dashed), $T_{\psi\psi}$ (dot dashed), and $T_{\theta\theta}$ (thick). For each of these, we have scaled our solution by C^{-1} defined below Eq. (3.10). Notably, each of these components is regular at the outer horizon (labeled by the vertical line at $r/r_c = 1$).

only included the part of the stress-energy tensor near $r = r_c$ because the behavior of the stress-energy tensor near the Cauchy horizon can be derived from (2.21) as was done for T_{rr} in (3.12). To verify that we obtained the correct holographic stress-energy tensor, we varied z_c between $(10^4\mu)^{1/5}$ and $(10^8\mu)^{1/5}$ and checked that $C^{-1}(T_{ab})$ did not change.

As pointed out for the nonrotating case, an interesting quantity is the energy density near the outer horizon. The local energy density may be found by diagonalizing the stress-energy tensor $(T^a{}_b)$, as done in [14]. The stress-energy tensor in our spacetime is diagonalizable near the horizon and far from the horizon, but there is an intermediate region

$$r_c\sqrt{1 - \kappa + \kappa^2 + (1-\kappa)\sqrt{1+\kappa^2}} < r$$
$$< r_c\sqrt{1 + \kappa + \kappa^2 + (1+\kappa)\sqrt{1+\kappa^2}} \qquad (4.7)$$

where the stress-energy tensor diagonalization breaks down. This is likely a result of our expansion, as in a fully nonperturbative solution like [14], no such region was seen, though it is notable that our solution contains a finite temperature, rather than extremal, bulk horizon. Following [14], in the region where this decomposition is well defined, we may write

$$T^a{}_b t^b = -\mathcal{E}(r)t^a, \qquad (4.8)$$

where t^a is the (unique) normalized timelike eigenvector, and $\mathcal{E}(r)$ can be interpreted as the energy density observed by the timelike observer with velocity t^a. At leading order in r and z_c,

$$t = \frac{1}{z_c}\left[\left(1 - 2\frac{(1+\kappa^2)r_c^2}{r^2} \pm \frac{\kappa^2 r_c^4}{r^4}\right)\frac{\partial}{\partial v} - \frac{\kappa\sqrt{1+\kappa^2}\,r_c^3}{r^4}\frac{\partial}{\partial \psi}\right]$$
$$+ \mathcal{O}\left(\frac{1}{r^5}, \frac{\mu^5}{z_c^5}\right). \qquad (4.9)$$

The plus sign in this equation corresponds to the near horizon region, while the minus sign corresponds to the region far from the horizon.

The energy density obtained from the decomposition is plotted in Fig. 3 for different values of κ. Just as in the nonrotating case, the region of negative energy density extends all the way from the horizon to spatial infinity. Interestingly, at spatial infinity, the energy density approaches a constant,

$$\mathcal{E}_\infty \equiv \lim_{r\to\infty}\mathcal{E}(r) = \epsilon^2 \cdot \frac{4C}{z_c^2} + \mathcal{O}(r^{-2}). \qquad (4.10)$$

This should not be surprising because far from the boundary black hole, the CFT should be in a thermal state, with an energy density corresponding to the temperature of the bulk black hole. In fact, this value matches the energy density for a CFT dual to a six-dimensional planar-AdS–Schwarzschild black brane. Furthermore, this value is independent of κ as it should be, since our boundary black holes are asymptotically flat, and a similar result was seen for $\kappa = 0$ in [12]. In Fig. 3, we have subtracted this asymptotic value from the energy density to emphasize that a local observer near the black hole measures an energy density less than the thermal energy density because of quantum effects in the curved background spacetime.

Interestingly, our energy density approaches $\mathcal{E}_\infty$ as r^{-2}, rather than the r^{-7} decay observed in [14]. This less steep
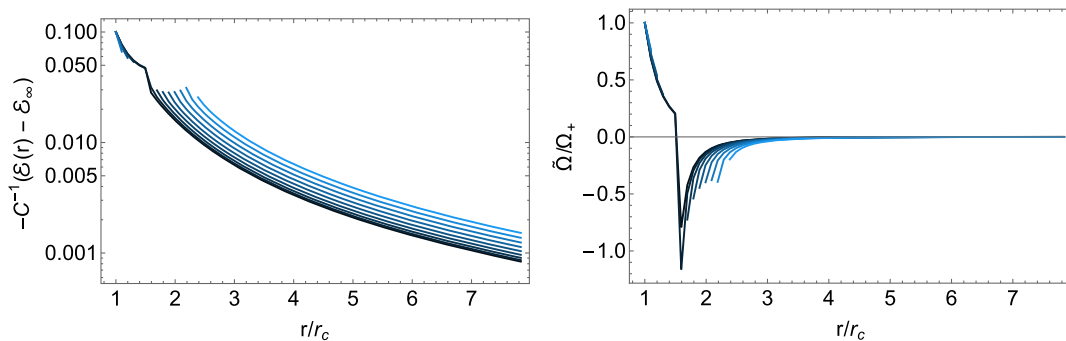

FIG. 3. (Left) Here we plot $\mathcal{E}(r)$ near the outer horizon for $\kappa = 0.1, 0.2, 0.3, 0.4, 0.5, 0.6, 0.7, 0.8, 0.9$ with $r_c = 0.1$, $\mu = 1$, $z_c = (10^8\mu)^{1/5}$. The color of the curves gets lighter as κ increases. As before, we have scaled the energy density by C^{-1} and set $\theta = \pi/2$. The upper left of the figure corresponds to the near horizon region. The curves are discontinuous because there is a region set by κ outside the event horizon [Eq. (4.7)], where the stress-energy tensor is not diagonalizable. (Right) Here we plot the rotation $\tilde{\Omega}(r)$ for the same values of κ. At the outer horizon, the rotation matches the value $\Omega(r_c, z_c)$ showing that t is the generator for the outer horizon. As before, discontinuities arise because the stress-energy tensor is not diagonalizable.
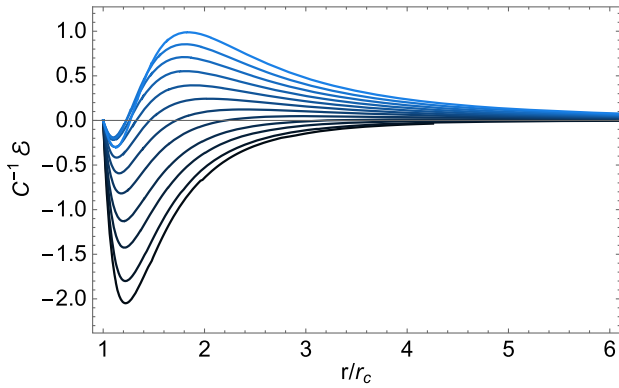
FIG. 4. The energy density seen by an observer with the tangent vector in Eq. (4.13). Here, we choose $\kappa = 0.02, 0.05, 0.1, 0.15, 0.2, 0.25, 0.3, 0.35, 0.4, 0.45, 0.5, 0.55$ and $r_c = 0.1$, $\mu = 1$, $z_c = 10\mu^{1/5}$. The color of the curves gets lighter as κ increases. For all κ, the energy density is negative near the outer horizon.

$$T = \frac{\partial}{\partial v} + \tilde{\Omega}(r, z)\frac{\partial}{\partial \psi} \qquad (4.11)$$

and define $\tilde{\Omega}$ to be the rotation. At the outer horizon, this becomes (at zeroth order in ϵ)

$$T_+ = \frac{\partial}{\partial v} + \sqrt{F(z_c)}\Omega(r_c, z_c)\frac{\partial}{\partial \psi}, \qquad (4.12)$$

which, on the conformal boundary, matches the future generator of the horizon at $r = r_c$. Note that the rotation decays as r^{-4} rather than the r^{-2} falloff seen in [14]. The faster falloff could again be a consequence of our perturbative expansion, though more likely a result of the droplet ending on a finite temperature bulk horizon.

To better understand the energy density in regions of the spacetime where $T^a{}_b$ is not diagonalizable, we instead define a new vector, timelike everywhere outside the outer horizon,

$$K = \frac{\partial}{\partial v} + \sqrt{F(z)}\Omega(r, z)\frac{\partial}{\partial \psi}, \qquad (4.13)$$

which also approaches T_+ at the outer horizon and goes to $(\partial/\partial v)$ near spatial infinity. An observer with this tangent vector would see the energy density plotted in Fig. 4, which is regular everywhere and still has the important feature of being negative near the event horizon. Furthermore, the localization of negative energy density near the event horizon is reminiscent of [15] and illuminates the "jammed" nature of the dual CFT. Here too, because $K \to \partial/\partial_v$ near spatial infinity, the energy density also approaches $\mathcal{E}_\infty$, indicative of the CFT in a thermal phase. This tangent vector, however, becomes spacelike inside the outer event horizon, and so is not useful to illustrate strong cosmic censorship. In this region, t^a is well defined and diverges on the Cauchy horizon.

falloff could be a consequence of our derivative expansion method. However, it is also notable that our droplet solution ends on a finite temperature black brane horizon, whereas in [14], the bulk horizon was extremal (the Poincaré horizon), and the black droplet was disconnected. Similar falloff discrepancies were seen in numerical constructions of five-dimensional static droplets, where the energy density decayed as r^{-5} with an extremal bulk horizon [21] but as r^{-1} for a finite temperature bulk horizon [22]. Importantly, as in the analytic case, for an observer with tangent vector t^a, for all choices of κ, the energy density diverges negatively as $(r - \kappa r_c)^{-2}$ near the Cauchy horizon.

We also can use the stress-energy tensor eigenvalue decomposition to define rotation of the dual plasma. Again, following [14], we write the timelike eigenvector of the stress-energy tensor as
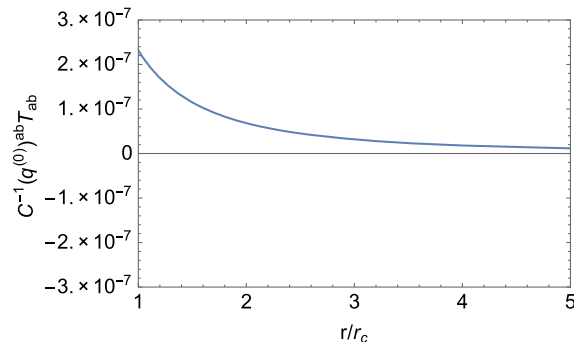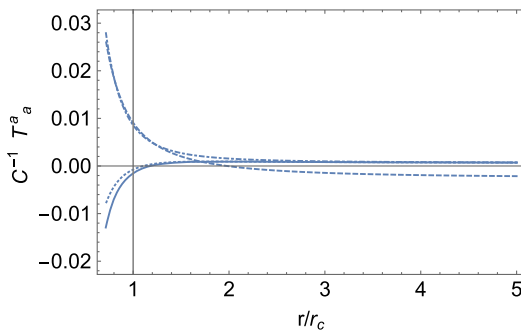

FIG. 5. The left plot displays the diagonal components of the holographic stress-energy tensor $T^a{}_a$ for $r_c = 0.1$, $k = 0.2$, $\mu = 1$, $z_c = (10^8\mu)^{1/5}$. The curves correspond to $T^\theta{}_\theta = T^\phi{}_\phi$ (dotted), $T^v{}_v$ (dashed), $T^r{}_r$ (dot dashed), $T^\psi{}_\psi$ (thick). Again, the vertical grey line indicates the outer event horizon. The right plot displays the sum of these components. Notably, the trace of the stress-energy tensor vanishes as $\mathcal{O}((\mu/z_c)^{10})$.

We emphasize that while the stress-energy tensor diverges on the Cauchy horizon, it is finite at $r = r_c$ so that it is regular on the past and future event horizons (shown in Fig. 2). Finally, one can check that the trace of the stress-energy tensor vanishes at leading order, as expected for a CFT in odd spacetime dimensions, just as in the nonrotating case. In Fig. 5, we have plotted the diagonal components of the holographic stress-energy tensor $C^{-1}(T^a{}_a)$ (no sum) as well as the trace. From this figure, it is clear that the sum vanishes as we approach the conformal boundary (i.e., $z_c \to \infty$). One can also check explicitly from the definition of the stress-energy tensor (3.9) and the equations of motion for $h_{\mu\nu}$ [(2.14)–(2.17)] that the trace vanishes as $\mathcal{O}((\mu/z_c)^{10})$ exactly following the nonrotating case.

To summarize our numerical results, for generic rotation parameter κ of our boundary black hole, the CFT plasma exhibits the following features. The stress-energy tensor is traceless to leading order in μ/z_c and regular on the outer event horizon. For a timelike observer, there is a region near the event horizon which has negative energy density. As a timelike observer approaches spatial infinity, the energy density seen by such an observer approaches that of the thermal CFT dual to a six-dimensional planar-AdS–Schwarzschild black brane. Depending on the observer's velocity, the energy density may remain less than this asymptotic value for all of space, as for the observer with tangent vector t^a, or there may be a region with positive energy density, as in the observer with tangent vector K. In all cases, this negative energy density diverges on the Cauchy horizon, as shown in Eq. (3.12), in favor of strong cosmic censorship.

V. CONCLUSION AND DISCUSSION

In this paper, we have analytically constructed a rotating black droplet solution embedded in the planar Schwarzschild-AdS black brane spacetime by applying the generalized derivative expansion method, which was originally developed for the static case [16]. Our method is valid when the horizon size of the black droplet is much smaller than the horizon size of the planar Schwarzschild-AdS black brane (and the curvature radius of the background AdS space). In this case, the derivative of the metric along the bulk radial direction z is much smaller than the one along the droplet radial direction r (parallel to the planar horizon). Then, order by order in the derivative expansion, we have been able to solve the Einstein equations. The horizon radius of the thin black droplet solution gradually shrinks toward the planar horizon and caps off smoothly just at the horizon. Since the temperature of the black droplet solution is much higher than the temperature of the background planar horizon, the dual

boundary state can be interpreted as the Unruh state [12]. For our black droplet solution, we have—analytically and holographically—computed the null-null components of the stress-energy tensor for a strongly coupled CFT in the boundary five-dimensional rotating Myers-Perry black hole spacetime. First, we have found that the negative energy appears just outside the event horizon, which can be interpreted as a consequence of the particle production by the Hawking effect. We have shown, however, there is no energy flux at infinity, as in the static case studied in [12], and, therefore, our boundary CFT can be viewed as a jammed state. We have also studied the behavior of the holographic stress-energy tensor near the inner Cauchy horizon. The null-null component of the stress-energy tensor corresponds to the energy density seen by an observer whose world line is transverse to the Cauchy horizon. We have found that the null-null component negatively diverges at the Cauchy horizon, suggesting that due to quantum effects, the Cauchy horizon would become singular, in favor of strong cosmic censorship.

Although we have not analyzed the classical instability of our droplet solution in the present paper, we expect our solution to show a classical instability or divergence of curvature scalars inside the event horizon. In fact, it was shown in [23] that, in general, adding stationary but spatially inhomogeneous linear perturbations makes inhomogeneous black branes unstable, rendering the Kretschmann scalar with respect to the perturbed geometry divergent on the Cauchy horizon. Viewing our black droplet solution as a type of inhomogeneous black string in the bulk and applying the general argument of [23], our droplet solution should also exhibit the divergence of curvature scalars at the Cauchy horizon even inside the bulk $z < z_c$. In the spirit of the bulk-boundary duality, our result of the quantum divergence of the stress-energy tensor at the Cauchy horizon in the boundary geometry may be viewed as a holographic realization of the classical divergence of curvatures at the Cauchy horizon in the bulk geometry.

APPENDIX: EXPRESSIONS
FOR $\mathcal{P}(r)$, $\mathcal{S}(r)$, $\mathcal{R}(r)$, AND $\mathcal{Q}(r)$

We provide the explicit expressions for $\mathcal{P}(r)$, $\mathcal{S}(r)$, $\mathcal{R}(r)$, and $\mathcal{Q}(r)$ appearing in (2.14)–(2.17),

$$
\begin{aligned}
\mathcal{P}(r) = {} & -2F_c^2 z_c^{10}(r^4 + \kappa^2 r_c^4)^3 r^2 - 5[-2r^{14} + r^{12}(r_c^2(1+\kappa^2) + 2\sqrt{r^4 + \kappa^2 r_c^4}) \\
& + 3\kappa^4 r_c^8 r^4 (r_c^2(1+\kappa^2) + 2\sqrt{r^4 + \kappa^2 r_c^4}) + \kappa^6 r_c^{12}(r_c^2(1+\kappa^2) + 3\sqrt{r^4 + \kappa^2 r_c^4}) \\
& + \kappa^2 r_c^4 r^8 (3r_c^2(1+\kappa^2) + 5\sqrt{r^4 + \kappa^2 r_c^4}) - r_c^2 r^{10}(6r_c^2\kappa^2 + (1+\kappa^2)\sqrt{r^4 + \kappa^2 r_c^4}) \\
& - r_c^6 r^6 \kappa^2(6r_c^2\kappa^2 + (1+\kappa^2)\sqrt{r^4 + \kappa^2 r_c^4}) - 2r_c^{10}\kappa^4 r^2(r_c^2\kappa^2 + 3(1+\kappa^2)\sqrt{r^4 + \kappa^2 r_c^4})]\mu^{10} \\
& + 2F_c z_c^5(r^4 + \kappa^2 r_c^4)[-6r^8\sqrt{r^4 + \kappa^2 r_c^4}\mu^5 - 9r^4\kappa^2 r_c^4\sqrt{r^4 + \kappa^2 r_c^4}\mu^5 - 3r_c^8\kappa^4\sqrt{r^4 + \kappa^2 r_c^4}\mu^5 \\
& + r^{10}(z_c^5 + 5\mu^5) + r^2 r_c^6 \kappa^2\{6(1+\kappa^2)\sqrt{r^4 + \kappa^2 r_c^4}\mu^5 + r_c^2\kappa^2(z_c^5 + 5\mu^5)\} \\
& + r^6 r_c^2\{3(1+\kappa^2)\sqrt{r^4 + \kappa^2 r_c^4}\mu^5 + 2r_c^2\kappa^2(z_c^5 + 5\mu^5)\}],
\end{aligned}
\tag{A1}
$$

$$
\begin{aligned}
\mathcal{S}(r) = {} & \frac{10\kappa\sqrt{1 + \kappa^2}\, r_c^3 r^2}{z_c^6}[2F_c^2 z_c^{10} r^2(r^4 + \kappa^2 r_c^4)^3 + 5\{-3r^{14} + 2(1+\kappa^2)r_c^2 r^{12} + 2\kappa^4(1+\kappa^2)r_c^{10}r^4 \\
& - \kappa^6\sqrt{r^4 + \kappa^2 r_c^4}r_c^{12} + \kappa^2 r_c^4(4(1+\kappa^2)r_c^2 + 5\sqrt{r^4 + \kappa^2 r_c^4})r^8 + r_c^2(-5r_c^2\kappa^2 + (1+\kappa^2)\sqrt{r^4 + \kappa^2 r_c^4})r^{10} \\
& + r_c^{10}\kappa^4(r_c^2\kappa^2 + 2(1+\kappa^2)\sqrt{r^4 + \kappa^2 r_c^4})r^2 - r_c^6\kappa^2(r_c^2\kappa^2 + 5(1+\kappa^2)\sqrt{r^4 + \kappa^2 r_c^4})r^6\}\mu^{10} \\
& + 2F_c z_c^5\{6\sqrt{r^4 + \kappa^2 r_c^4}\mu^5 r^{12} + 7r_c^4\kappa^2\sqrt{r^4 + \kappa^2 r_c^4}\mu^5 r^8 - r_c^{12}\kappa^6\sqrt{r^4 + \kappa^2 r_c^4}\mu^5 - (z_c^5 + 5\mu^5)r^{14} \\
& + r_c^{10}\kappa^4(2(1+\kappa^2)\sqrt{r^4 + \kappa^2 r_c^4}\mu^5 - r_c^2\kappa^2(z_c^5 - 3\mu^5))r^2 \\
& + r_c^6\kappa^2(-5(1+\kappa^2)\sqrt{r^4 + \kappa^2 r_c^4}\mu^5 - r_c^2\kappa^2(3z_c^5 - \mu^5))r^6 \\
& - r_c^2(3(1+\kappa^2)\sqrt{r^4 + \kappa^2 r_c^4}\mu^5 + r_c^2\kappa^2(3z_c^5 + 7\mu^5))r^{10}\}],
\end{aligned}
\tag{A2}
$$

$$
\begin{aligned}
\mathcal{R}(r) = {} & \frac{10\kappa^2 r_c^4 r}{z_c^6}[2F_c^2 z_c^{10} r^2(r^4 + \kappa^2 r_c^4)^2(5r^4 + \kappa^2 r_c^4) + 5\{4r_c^{10}\kappa^4(1+\kappa^2)r^4 - \kappa^6 r_c^{12}\sqrt{r^4 + \kappa^2 r_c^4} \\
& + 5r_c^2(1+\kappa^2)\sqrt{r^4 + \kappa^2 r_c^4}r^{10} - 5r_c^6\kappa^2(1+\kappa^2)\sqrt{r^4 + \kappa^2 r_c^4}r^6 + 2r_c^{10}\kappa^4(1+\kappa^2)\sqrt{r^4 + \kappa^2 r_c^4}r^2 \\
& + (4r_c^2(1+\kappa^2) - 6\sqrt{r^4 + \kappa^2 r_c^4})r^{12} + \kappa^2 r_c^4(8r_c^2(1+\kappa^2) + 3\sqrt{r^4 + \kappa^2 r_c^4})r^8\}\mu^{10} \\
& - 2F_c z_c^5\{-6\sqrt{r^4 + \kappa^2 r_c^4}\mu^5 r^{12} - 7r_c^4\kappa^2\sqrt{r^4 + \kappa^2 r_c^4}\mu^5 r^8 + r_c^{12}\kappa^6\sqrt{r^4 + \kappa^2 r_c^4}\mu^5 + (5z_c^5 + \mu^5)r^{14} \\
& + \kappa^2 r_c^6\{5(1+\kappa^2)\sqrt{r^4 + \kappa^2 r_c^4}\mu^5 + r_c^2\kappa^2(7z_c^5 - 5\mu^5)\}r^6 \\
& + \kappa^4 r_c^{10}\{-2(1+\kappa^2)\sqrt{r^4 + \kappa^2 r_c^4}\mu^5 + r_c^2\kappa^2(z_c^5 - 3\mu^5)\}r^2 \\
& + r_c^2\{3(1+\kappa^2)\sqrt{r^4 + \kappa^2 r_c^4}\mu^5 + r_c^2\kappa^2(11z_c^5 - \mu^5)\}r^{10}\}],
\end{aligned}
\tag{A3}
$$

$$\mathcal{Q}(r) = \frac{5\mu^5 r^2}{z_c^6}[6(2z_c^5 + 3\mu^5)r^{16} - 2\kappa^6(1 + \kappa^2)r_c^{14}(2z_c^5 + 3\mu^5)\sqrt{r^4 + \kappa^2 r_c^4}$$

$$- r_c^8\kappa^2(1 + \kappa^2)\{10(1 + \kappa^2)(2z_c^5 + 3\mu^5)\sqrt{r^4 + \kappa^2 r_c^4} + r_c^2\kappa^2(8z_c^5 + 7\mu^5)\}r^6$$

$$- 3\{2(2z_c^5 + 3\mu^5)\sqrt{r^4 + \kappa^2 r_c^4} + r_c^2(1 + \kappa^2)(8z_c^5 + 7\mu^5)\}r^{14}$$

$$+ \kappa^4 r_c^{12}\{(4 + 9\kappa^2 + 4\kappa^4)(2z_c^5 + 3\mu^5)\sqrt{r^4 + \kappa^2 r_c^4} + r_c^2\kappa^2(1 + \kappa^2)(8z_c^5 + 7\mu^5)\}r^2$$

$$- r_c^4\{5r_c^2\kappa^2(1 + \kappa^2)(8z_c^5 + 7\mu^5) + \sqrt{r^4 + \kappa^2 r_c^4}\{2z_c^5(6 + 19\kappa^2 + 6\kappa^4) + (-2 + 17\kappa^2 - 2\kappa^4)\mu^5\}\}r^{10}$$

$$+ 5r_c^2\{3(1 + \kappa^2)(2z_c^5 + \mu^5)\sqrt{r^4 + \kappa^2 r_c^4} + 2r_c^2(2z_c^5\kappa^2 + (1 + 5\kappa^2 + \kappa^4)\mu^5)\}r^{12}$$

$$- 2r_c^{10}\kappa^4\{(1 + \kappa^2)(2z_c^5 + 3\mu^5)\sqrt{r^4 + \kappa^2 r_c^4} + r_c^2(2z_c^5\kappa^2 - (5 + 7\kappa^2 + 5\kappa^4)\mu^5)\}r^4$$

$$+ r_c^6\kappa^2\{(1 + \kappa^2)(38z_c^5 + 47\mu^5)\sqrt{r^4 + \kappa^2 r_c^4} + 2r_c^2(2z_c^5\kappa^2 + (10 + 23\kappa^2 + 10\kappa^4)\mu^5)\}r^8]. \tag{A4}$$

[1] L. H. Ford, M. J. Pfenning, and T. A. Roman, Quantum inequalities and singular negative energy densities, Phys. Rev. D **57**, 4839 (1998).

[2] W. A. Hiscock, Stress-energy tensor near a charged, rotating, evaporating black hole, Phys. Rev. D **15**, 3054 (1977).

[3] W. A. Hiscock and D. A. Konkowski, Quantum vacuum energy in Taub-NUT (Newman-Unti-Tamburino)-type cosmologies, Phys. Rev. D **26**, 1225 (1982).

[4] J. Maldacena The large N limit of superconformal field theories and supergravity, Adv. Theor. Math. Phys. **2**, 231 (1998); O. Aharony, S. Gubser, J. Maldacena, H. Ooguri, and Y. Oz, Large N field theories, string theory and gravity, Phys. Rep. **323**, 183 (2000).

[5] V. E. Hubeny, D. Marolf, and M. Rangamani, Hawking radiation in large N strongly-coupled field theories, Classical Quantum Gravity **27**, 095015 (2010).

[6] V. E. Hubeny, D. Marolf, and M. Rangamani, Hawking radiation from AdS black holes, Classical Quantum Gravity **27**, 095018 (2010).

[7] V. E. Hubeny, D. Marolf, and M. Rangamani, Black funnels and droplets from the AdS C-metrics, Classical Quantum Gravity **27**, 025001 (2010).

[8] M. M. Caldarelli, O. J. C. Dias, R. Monteiro, and J. E. Santos, Black funnels and droplets in thermal equilibrium, J. High Energy Phys. 05 (2011) 116.

[9] S. Fischetti, D. Marolf, and J. E. Santos, AdS flowing black funnels: Stationary AdS black holes with non-Killing horizons and heat transport in the dual CFT, Classical Quantum Gravity **30**, 075001 (2013).

[10] S. Fischetti and D. Marolf, Flowing funnels: Heat sources for field theories and the AdS$_3$ dual of CFT$_2$ Hawking radiation, Classical Quantum Gravity **29**, 105004 (2012).

[11] J. E. Santos and B. Way, Black funnels, J. High Energy Phys. 12 (2012) 060.

[12] N. Haddad, Hawking radiation from small black holes at strong coupling and large N, Classical Quantum Gravity **30**, 195002 (2013).

[13] S. Fischetti and J. E. Santos, Rotating black droplet, J. High Energy Phys. 07 (2013) 156.

[14] P. Figueras and S. Tunyasuvunakool, CFTs in rotating black hole backgrounds, Classical Quantum Gravity **30**, 125015 (2013).

[15] E. Mefford, Entanglement entropy in jammed CFTs, arXiv:1605.09369.

[16] N. Haddad, Black strings ending on horizons, Classical Quantum Gravity **29**, 245001 (2012).

[17] R. Emparan, T. Harmark, V. Niarchos, and N. A. Obers, World-Volume Effective Theory for Higher-Dimensional Black Holes, Phys. Rev. Lett. **102**, 191301 (2009).

[18] J. Armas, How Fluids Bend: the Elastic Expansion for Higher-Dimensional Black Holes, J. High Energy Phys. 09 (2013) 073.

[19] R. C. Myers and M. Perry, Black holes in higher dimensional space-times, Ann. Phys. (N.Y.) **172**, 304 (1986).

[20] R. Emparan, C. V. Johnson, and R. C. Myers, Surface terms as counterterms in the AdS/CFT correspondence, Phys. Rev. D **60**, 104001 (1999).

[21] P. Figueras, J. Lucietti, and T. Wiseman, Ricci solitons, Ricci flow, and strongly coupled CFT in the Schwarzschild Unruh or Boulware vacua, Classical Quantum Gravity **28**, 215018 (2011).

[22] J. E. Santos and B. Way, Black droplets, J. High Energy Phys. 08 (2014) 072.

[23] K. Maeda, T. Okamura, and J. I. Koga, Inhomogeneous charged black hole solutions in asymptotically anti–de Sitter spacetime, Phys. Rev. D **85**, 066003 (2012).